J Neurophysiol 96: 3220–3230, 2006.
First published September 27, 2006; doi:10.1152/jn.00110.2006.

Nonuniform Distribution of Reach-Related and Torque-Related Activity in Upper Arm Muscles and Neurons of Primary Motor Cortex

Isaac Kurtzer, Troy M. Herter, and Stephen H. Scott
Department of Anatomy and Cell Biology, Canadian Institute of Health Research Group in Sensory-Motor Systems, Centre for Neuroscience Studies, Queen's University, Kingston, Canada

Submitted 1 February 2006; accepted in final form 16 September 2006

Kurtzer, Isaac, Troy M. Herter, and Stephen H. Scott. Nonuniform distribution of reach-related and torque-related activity in upper arm muscles and neurons of primary motor cortex. *J Neurophysiol* 96: 3220–3230, 2006. First published September 27, 2006; doi:10.1152/jn.00110.2006. The present study examined the activity of primate shoulder and elbow muscles using a novel reaching task. We enforced similar patterns of center-out movement while the animals countered viscous loads at their shoulder, elbow, both joints, or neither joint. Accordingly, we could examine reach-related activity during the unloaded condition and torque-related activity by comparing activity across load conditions. During unloaded reaching the upper arm muscles exhibited a bimodal distribution of preferred hand direction. Maximal reach-related activity occurred with hand movements mostly toward or away from the body. Arm muscles also exhibited a bimodal distribution of their preferred torque direction. Maximal torque-related activity typically occurred with shoulder-extension/elbow-flexion torque or shoulder-flexion/elbow-extension torque. Similar biases in reach-related and torque-related activity could be reproduced by optimizing a global measure of muscle activity. These biases were also observed in the neural activity of primary motor cortex (M1). The parallels between M1 and muscular activity demonstrate another link between motor cortical processing and the motor periphery and may reflect an optimization process performed by the sensorimotor system.

INTRODUCTION

Motor coordination reflects a complex interaction between behavioral goals, neural function, and the musculoskeletal apparatus (Loeb et al. 1999; Scott 2004; Todorov 2000). This complexity is exemplified by the dissociation of a muscle's function and anatomical action (Buchanan et al. 1989; Hoffman and Strick 1999; Jongen et al. 1989; Nozaki et al. 2005; van Zuylen et al. 1988). For example, the elbow extensor triceps brachii lacks any mechanical action at the wrist but is recruited during wrist supination to counter the elbow flexor torque of biceps brachii, an elbow flexor and wrist supinator (Buchanan et al. 1989). Although wrist supination could be produced using only single-joint muscles (supinators) the nervous system uses all muscles with supinating action, even those acting at multiple joints or having multiple degrees of freedom at a single joint. A similar strategy is predicted by models that optimize a global measure of muscle activity (Collins et al.1995; Crowninshield and Brand 1981; Dul et al. 1984; Fagg et al. 2002; van Bolhuis and Gielen 1999).

We recently observed a similar dissociation of muscle function and action in an animal model of postural control (Kurtzer et al. 2006). Monkeys trained to maintain a constant arm posture recruited their shoulder monoarticulars when countering elbow loads and elbow monoarticulars when countering shoulder loads. These single-joint muscles were most active when producing shoulder-extension/elbow-flexion torque and shoulder-flexion/elbow-extension torque consistent with the optimization of muscle activity.

Inferring the function of muscular activity during movement is considerably more complicated. The limb's intersegmental dynamics allow single-joint motion to arise from multijoint torque and multijoint motion to arise from single-joint torque (Graham et al. 2003a; Hollerbach and Flash 1982; Zajac and Gordon 1989). Moreover, a muscle's ability to generate force strongly depends on its length and velocity (Joyce et al. 1969; Scott et al. 1996). These complexities can be addressed by calculating the inverse dynamics associated with movement and using a muscle model. Another approach is to experimentally enforce similar movement patterns under different load conditions (van Bolhuis et al. 1998). Thereby, one can "factor out" the complex transformation of muscle activity to joint torque and relate the difference in activity specifically to the difference in load between conditions, i.e., torque-related activity.

The present study used a loaded-reach paradigm to examine muscular activity during center-out planar reaching. Similar reaching patterns were enforced while a robotic exoskeleton applied mechanical loads at the shoulder, elbow, both, or neither joint. During the unloaded condition, we observed that upper limb muscles were primarily activated during movements either toward the body or away from the body (i.e., the fore–aft axis). This strong bias was not observed in earlier studies that used handheld manipulanda and less constrained arm movements, but is prominent during the more controlled conditions we used. Comparing muscular activity across the load conditions revealed a bias in torque-related activity toward shoulder-extension/elbow-flexion torque and shoulder-flexion/elbow-extension torque. Although dissociations between muscular function and anatomy have been observed during posture (Buchanan et al. 1989; Jongen et al. 1989; Nozaki et al. 2005) and movement tasks (Hoffman and Strick 1999) this is the first movement task that experimentally controlled for the activity during unloaded reaching. Moreover,

Address for reprint requests and other correspondence: S. H. Scott, Centre for Neuroscience Studies, Botterell Hall, Rm 232, Queen's University, Kingston, Ontario, K7L 3N6, Canada (E-mail: steve@biomed.queensu.ca).

The costs of publication of this article were defrayed in part by the payment of page charges. The article must therefore be hereby marked "*advertisement*" in accordance with 18 U.S.C. Section 1734 solely to indicate this fact.

we reproduced these reach-related and torque-related biases with a model that optimized a global measure of muscle activity.

Such data are not only valuable for understanding how muscles are used for motor function, but also provide a foundation for interpreting how regions like primary motor cortex (M1) are involved in controlling movement. M1 is the principal cortical region supporting voluntary motor execution and has a strong association with the motor periphery in its somatosensory input and segmental output (Hepp-Reymond 1988; Porter and Lemon 1993; Scott 2003). In fact, here we report that arm-related M1 neurons recorded from the same monkeys exhibited both a reach-related bias and a torque-related bias similar to those of the arm muscles. Thus we provide a link between behavioral goals, neural function, and the musculoskeletal apparatus during planar reaching.

METHODS

Task and apparatus

Four male rhesus monkeys (*Macaca mulatta*, 6–12 kg) performed upper limb motor tasks according to guidelines of the Queen's University Animal Care Committee. The monkey's right forelimb was supported by a robotic exoskeleton (KINARM; BKIN Technologies, Kingston, Ontario, Canada) that permitted horizontal shoulder and elbow motion, monitored those joint motions, and could apply mechanical loads to the two joints (Scott 1999). This mechanical system was coupled to a virtual reality display so that monkeys viewed their entire limb and visual targets in the horizontal plane of movement.

The task involved center-out movements of the monkey's right forelimb (Fig. 1*A*). Hand movements were initiated near the center of the hand's workspace (about 30° shoulder angle and 90° elbow angle) where the passive stiffness of the limb was relatively small (Graham et al. 2003b). Peripheral targets were 1.2 cm wide and spaced 6.0 cm from the central target. The different monkeys were exposed to different targets as follows. Monkeys A and B reached to eight targets distributed roughly uniformly in joint-torque space, but unevenly in hand space: 45, 67.5, 90, 180, 247.5, 270, 315, and 337.5°, where 0° is to the right and positive rotation is anticlockwise. In contrast, monkeys C and D reached to eight targets distributed uniformly in hand space: 0, 45, 90, 135, 180, 225, 270, and 315°.

During reaching motions the KINARM imposed a positive viscous load (0.2 $N \cdot m \cdot s \cdot rad^{-1}$) at the shoulder, elbow, both, or neither joint. Simply put, the applied load opposed motion at the shoulder, elbow, both, or neither joint proportional to the angular velocity at that joint. Monkeys A and B reached to all targets during the unloaded and three viscous load conditions. Monkey C reached to eight targets during the unloaded condition and two targets (90 and 270°) during three viscous load conditions. Last, monkey D reached to eight targets during the unloaded and viscous-both conditions. Monkey D was not exposed to the viscous shoulder and viscous elbow conditions.

Targets were presented randomly within a block of the same load condition. This pseudorandom block design allowed stable performance after the first reach to each target that was excluded from the analysis. Blocks were repeated six times (monkeys A, B, and D) or ten times (monkey C) for a total of 48 or 20 trials. Further, similar hand trajectories were implicitly enforced across the different load conditions by requiring temporal and spatial accuracy. The monkey's hand had to move between the start and peripheral radii within 220–350 ms. Note that that hand's acceleration/deceleration within these target radii led to total movement times within 500–600 ms.

Muscle recording

Electromyographic (EMG) activity was recorded with both acute and chronic techniques (Kurtzer et al. 2006; Loeb and Gans 1986; Scott and Kalaska 1997). Acute recordings (monkeys A–D) involved inserting two single-strand wires percutaneously into the muscle belly followed by microstimulation to verify the electrode placement. Chronic recordings (monkeys A and C) involved surgically implanting bipolar multistrand electrodes in the superficial portion of the muscle belly. For both techniques EMG signals were recorded (1,000 Hz for Monkey A; 4,000 Hz for monkeys B–D), full-wave rectified, and integrated into 5-ms bins.

EMG was collected from 11 different muscles. Each muscle could be sampled multiple times (maximum = 6) given the two monkeys with acute recordings only and two monkeys with both acute and chronic recordings. To be selected a muscle recording needed to score $\geq$3 on a subjective rating of signal quality between 1 (poor) and 5 (excellent) and also exhibit directionally tuned muscle activity during unloaded reaching (bootstrap, $P < 0.01$). Directionally tuned activity was determined with the plate method, a nonparametric technique for characterizing the "mass distribution" of activity (Gribble and Scott 2002a).

The 35 samples that met this criterion are shown in Table 1. Only four sample muscles had scores $\geq$3 but lacked significant directional tuning. These few samples—three biarticulars and one monoarticular—exhibited phasic modulation during the reaching period along with large modulation with the final limb position; the complex interaction was not captured by a simple measure of directional tuning.

Neural recording

Standard techniques were used for extracellular recordings in the shoulder/elbow region of M1 (Scott and Kalaska 1997; Scott et al. 2001). A general analysis of these data was previously reported

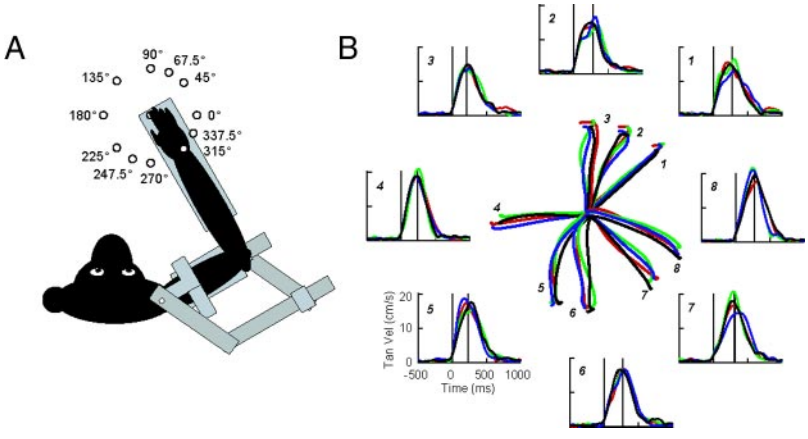

FIG. 1. Experimental arrangement. *A*: monkey is shown facing the targets with its hand at the start position and limb maintained in the horizontal plane by the KINARM; the monkey, apparatus, and targets are similarly scaled. Each monkey reached to a subset of the 11 targets shown (see METHODS). *B*: *center panel* depicts the mean hand paths of a sample session. *Peripheral panels* show the mean hand speed from the same session; vertical lines indicate the mean time of movement onset and peak velocity across load conditions. Different colors denote the different load conditions: unloaded (black), viscous shoulder (red), viscous elbow (green), and viscous both (blue).

TABLE 1. *Muscle samples*

Muscle Group	Muscle	Samples			
		Monkey, PHD (Unloaded Condition), PHD (Loaded Conditions)			
Shoulder extensor	Posterior Deltoid (DP) (expected PTD = **180**°)	Chronic:	A	PHD: 315°	PTD: 185 ± 7°
			C	PHD: 309°	PTD: 190 ± 18°
		Acute:	A	PHD: 313°	PTD: 186 ± 9°
			B	PHD: 319°	**PTD: 169 ± 7°**
			C	PHD: 287°	PTD: 160 ± 27°
			D	PHD: 290°	ns
Shoulder flexor	Anterior Deltoid (DA) (expected PTD = **0**°)	Chronic:	A	PHD: 130°	PTD: 9 ± 11°
			C	PHD: 121°	PTD: 346 ± 18°
		Acute:	A	PHD: 88°	**PTD: 296 ± 21°**
			C	PHD: 108°	PHD: 21 ± 25°
	Pectoralis Major (PM) (expected PTD = **0**°)	Chronic:	C	PHD: 147°	PTD: 1 ± 12°
		Acute:	B	PHD: 103°	*PTD: 14 ± 8°*
			C	PHD: 105°	ns
Elbow extensor	Triceps Lateral (Tla) (expected PTD = **270**°)	Acute:	B	PHD: 98°	PTD: 282 ± 16°
			D	PHD: 76°	**PTD: 314 ± 35°**
	Triceps Medial (Tme) (expected PTD = **270**°)	Acute:	A	PHD: 70°	**PTD: 282 ± 5°**
				PHD: 79°	**PTD: 282 ± 10°**
Elbow flexor	Brachialis (B) (expected PTD = **90**°)	Chronic:	A	PHD: 268°	**PTD: 111 ± 17°**
			C	PHD: 275°	**PTD: 115 ± 22°**
		Acute:	A	PHD: 269°	**PTD: 114 ± 5°**
			B	PHD: 281°	**PTD: 158 ± 18°**
			C	PHD: 273°	PTD: 89 ± 30°
			D	PHD: 251°	PTD: 122 ± 41°
	Brachioradialis (Br) (expected PTD = **90**°)	Chronic:	C	PHD: 248°	PTD: 99 ± 38°
		Acute:	B	PHD: 275°	**PTD: 130 ± 8°**
			D	PHD: 256°	ns
	Extensor Carpi Radialis Longus (ECRL) (expected PTD = **90**°)	Acute:	B	PHD: 285°	**PTD: 184 ± 13°**
			D	PHD: 265°	ns
Biarticular extensor	Triceps Long (Tlo) (expected PTD = **198**°)	Chronic:	A	PHD: 320°	**PTD: 164 ± 3°**
			C	PHD: 306°	**PTD: 174 ± 16°**
		Acute:	B	PHD: 290°	**PTD: 153 ± 8°**
Biarticular flexor	Biceps Long (BL) (expected PTD = **71**°)	Acute:	B	PHD: 269°	**PTD: 104 ± 16°**
			D	PHD: 229°	**PTD: 141 ± 46°**
	Biceps Short (BS) (expected PTD = **51**°)	Chronic:	A	PHD: 155°	ns
		Acute:	B	PHD: 245°	ns

The bold and italicized fonts indicate a significant PTD rotation toward and away from whole-arm flexion/whole-arm extension, respectively. See *inset* of Fig. 10.

(Gribble and Scott 2002b; Scott et al. 2001). Here we restrict our analyses to neurons that exhibited directionally tuned activity during unloaded reaching (bootstrap, $P < 0.01$) and were recorded during a load condition; 95 neurons from all four monkeys met the criteria.

Data analysis

HAND SPACE. Analyses focused on the period between movement onset (10% of the peak hand velocity) and peak hand velocity. Muscle activity was quantified as the mean rectified voltage from movement onset to peak hand velocity. Likewise, joint torque, joint position, and joint velocity were quantified as their mean values from movement onset to peak hand velocity. We examined M1 activity from 75 ms before movement onset to 75 ms before peak hand velocity to approximate the delay between M1 and muscular activity (Cheney and Fetz 1988; Morrow and Miller 2003). Neural activity was quantified as the mean spike rate in this time window.

We examined two aspects of hand kinematics–the peak tangential velocity of the hand and the direction of movement at peak velocity, to confirm similar movement patterns across load conditions. Movement similarity was tested between the loaded and unloaded conditions with one-way ANOVAs ($P < 0.01$) for each session.

Several analyses focused on the muscle and neural activity related to the hand motion during unloaded reaching, i.e., reach-related activity. The plate method determined the movement direction with maximal activity, i.e., the preferred hand direction (PHD). We examined the PHD for each sampled muscle and the average PHD of the six relevant muscle groups: shoulder flexors, shoulder extensors, elbow flexors, elbow extensors, biarticular flexors, and biarticular extensors. Note that this working definition of muscle group includes muscles with a similar mechanical action (Table 1).

We also determined whether the global trend of all muscular (or neural) PHDs was best described as one, two, or four symmetrically distributed clusters (Rayleigh test; Baschelet 1981). To test for a unimodal, bimodal, and quadrimodal distribution we multiplied the PHDs by 1, 2, or 4. Next, we summed the PHDs tip to tail and normalized by their absolute summed length. This transformation produces a mean vector whose length ranged from 0 to 1 for perfectly random to perfectly similar PHDs, i.e., a circular correlation. The orientation of this vector is the mean orientation of the distribution. Note that the resulting mean vector is not identical to the mode vector so that smaller subclusters remain unidentified. We used this same technique to examine the bimodal distribution [preferred hand axis (PHA)] of opposing kinematic/kinetic variables such as elbow flexor and extensor torque.

The PHD distributions of muscles and neurons were compared using a random bootstrap with replacement ($n = 1{,}000$). By repeatedly sampling each distribution's mean vector we estimated its 95% confidence interval. If the top or bottom 2.5% of the resampled means did not contain the "observed" mean of the other

distribution then the two distributions were considered significantly different at $P < 0.05$.

Another test examined the relative increase (MaxΔ) and decrease (MinΔ) from the prereach activity during unloaded reaching

$$(\text{Max}\Delta + \text{Min}\Delta)/(\text{Max}\Delta - \text{Min}\Delta)$$

This unloaded excitation–inhibition score (unloaded-EI) varied between −1 (pure inhibition), 0 (equal excitation and inhibition), and +1 (pure excitation). A Wilcoxon rank-sum compared the unloaded-EI scores from muscle and neurons.

TORQUE SPACE. A second set of analyses focused on the change in (muscular and neural) activity with respect to the change in joint torque between the unloaded and loaded conditions (i.e., torque-related activity). Joint torques at the shoulder and elbow were calculated using the equations of motion for a planar two-segment arm including the robotic exoskeleton (Scott 1999). Changes in shoulder and elbow joint torque were subsequently calculated as the difference in joint torque between loaded and unloaded conditions.

Torque-related activity was assessed by a planar regression (F-statistic, $P < 0.01$). This method can readily handle the nonuniform distribution of torque direction and torque magnitude that results from the nonuniform relation between hand motion, joint velocity, and joint torque (Graham et al. 2003b). The shoulder (S) and elbow (E) slope coefficients from the plane fit describe the relative sensitivity to shoulder and elbow joint torque–preferred torque direction, atan (E/S) (Cabel et al. 2001; Kurtzer et al. 2005). Preferred torque direction (PTD) was measured counterclockwise from shoulder flexion so shoulder flexor, elbow flexor, shoulder extensor, and elbow extensor PTDs occur at 0, 90, 180, and 270°, respectively.

Applying a separate planar regression to each repeat block assessed intertrial reliability of the PTDs. The circular correlation and number of blocks together define a 95% angular confidence interval about the measured PTD (Baschelet 1981). The measured PTD was compared with the anatomical action of a muscle as determined from a previous study (Graham et al. 2003a). If the anatomical action was outside the confidence interval, then the measured muscle PTD is considered significantly deviated from expectation.

Three additional statistics examined trends in torque-related activity: *1*) A Rayleigh's test determined whether the entire sample of PTDs had a significant unimodal, bimodal, or quadrimodal distribution (Baschelet 1981). *2*) A loaded excitation–inhibition score (loaded-EI score) determined whether load-related changes were primarily an increase or decrease from the activity during unloaded reaching. The different sets of loaded-EI scores were compared with a Wilcoxon rank-sum test. *3*) Bootstrap tests compared the PTDs of muscles and neurons.

Models of muscle activation

We examined several different models of muscle activation. These models included two parts: muscle properties and recruitment strategy. Muscle properties included the muscle's morphometry and intrinsic mechanics. We used a lumped representation for the six muscle groups using known values of the monkey's moment arms, fascicle lengths (l), and physiological cross-sectional area (PSCA) (Cheng and Scott 2000; Graham and Scott 2003b). Each lumped muscle group was represented four times, one for each monkey.

Muscle properties included passive stiffness and velocity-dependent force production. Stiffness was estimated as a one-sided cubic function (Graham et al. 2003a). Damping was estimated as a dissipating exponential for muscle shortening and saturating exponential for muscle lengthening (Scott et al. 1996). The mean joint kinematics for each condition and each monkey determined the length and velocity of the muscle fascicles of each muscle group.

The recruitment strategy determined how muscles were activated to achieve a target torque. The target torques for all models was the mean torque from movement onset to peak hand velocity measured for each condition and each monkey. We examined two basic recruitment strategies: "direct activation" and "optimal activation." The "direct activation" strategy recruited a muscle proportional to the angular similarity (dot-product) of the target torque and the muscle's moment arm. This strategy does not account for any interactions among muscles; i.e., it will not achieve the target torque when all muscles are activated. It is presented for didactic purposes.

The strategy of "optimal activation" achieved each target torque while minimizing a global measure of muscle activity; i.e., it accounts for interactions among muscles. We focused on one measure of muscle activity, the sum of muscle stress squared $\{[\text{sumn}](f_i/\text{PCSA}_i)^2\}$. "Optimal activation" was determined by an iterative procedure previously used for our posture task (Kurtzer et al. 2006). The procedure achieved each target torque under the constraint that muscles could only pull and the muscle parameters were constant (fmincon function, MATLAB; The MathWorks, Natick, MA). We analyzed the simulated activity of the models with the same tools used for our real data set.

RESULTS

Movement patterns and torque patterns

The animals' unloaded reaching movements exhibited the canonical pattern of gently curved hand trajectories with bell-shaped velocity profiles (Morasso 1981) (Fig. 1*B*). Hand paths showed minimal systematic curvature across all targets (Fig. 2*A*). Moreover, the hand velocities were largely similar across different targets (Fig. 2*B*). The slowest hand velocity across different targets was 80% of the fastest hand velocity; the slowest movements were often directed to targets near the

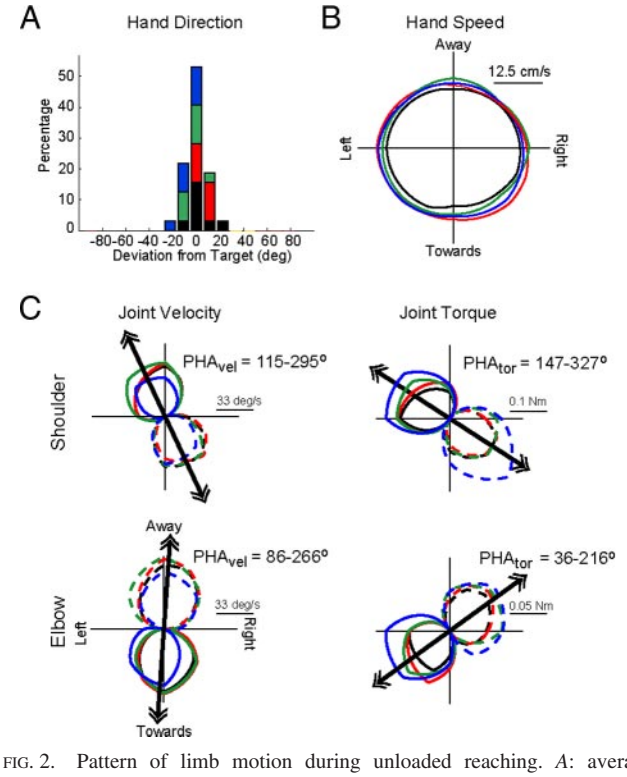

FIG. 2. Pattern of limb motion during unloaded reaching. *A*: average angular difference between the mean hand path and a straight line to the target. Different colors denote the 4 different monkeys in each panel. *B*: mean hand speed when reaching to different targets. *C*: spatial distribution of joint velocity and joint torque when reaching to different targets. Solid and dashed lines denote flexion and extension, respectively. Arrows indicate the mean bimodal distribution in hand space [preferred hand axis (PHA)].

fore–aft axis. This variation was within our strict requirement on temporal and spatial accuracy (see METHODS, *Task and apparatus*).

The similar hand movements were achieved by strong modulations in the underlying joint velocities and torques (Fig. 2*C*). The slowest joint velocity—(elbow velocity^2 + shoulder velocity^2)$^{1/2}$—across different targets was 27% of the fastest joint velocity. Likewise, the smallest joint torque—(elbow torque^2 + shoulder torque^2)$^{1/2}$—across different targets was 45% of the largest joint torque. The complex relation between joint mechanics and hand motion resulted in maximum joint velocity and displacement near the fore–aft axis (shoulder, bimodal PHA_{vel} = 115–295°; elbow, bimodal PHA_{vel} = 86–266°). In contrast, the maximum joint torque was weakly biased to the left–right axis (shoulder, bimodal PHA_{tor} = 147–327°; elbow, bimodal PHA_{tor} = 36–216°).

The described movement patterns were conserved across different load conditions; 90% of the individual loaded trials had a movement direction within 15° of the mean direction during unloaded trials (Fig. 3*A*). Likewise, 88% of the individual loaded trials had a peak velocity within 20% of the mean velocity during unloaded trials (Fig. 3*B*). Only 18 and 13% of the comparisons had significant differences in movement direction and peak velocity, respectively (one-way ANOVAs, $P < 0.01$).

The viscous loads required a range of compensatory torques proportional to the motion of the shoulder and/or elbow joint (Fig. 4, *A* and *B*). The maximum shoulder torque during the viscous-shoulder condition was roughly 150% of the unloaded maximum. Likewise, elbow torque during the viscous-elbow condition was roughly 200% of the unloaded maximum.

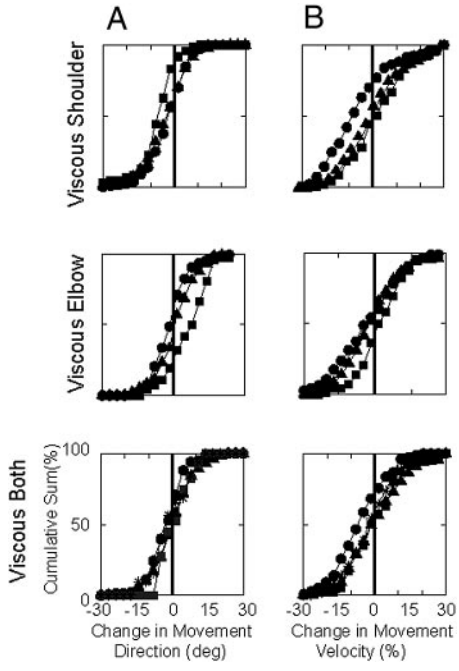

FIG. 3. Pattern of limb motion when reaching with different imposed loads. *A*: cumulative histograms show the change in initial movement direction between the unloaded and loaded conditions. *B*: change in peak hand velocity between loaded and unloaded conditions normalized to unloaded peak velocity. Data from the viscous shoulder, viscous elbow, and viscous both conditions are presented in descending order. Circles, squares, triangles, and stars denote monkeys A–D.

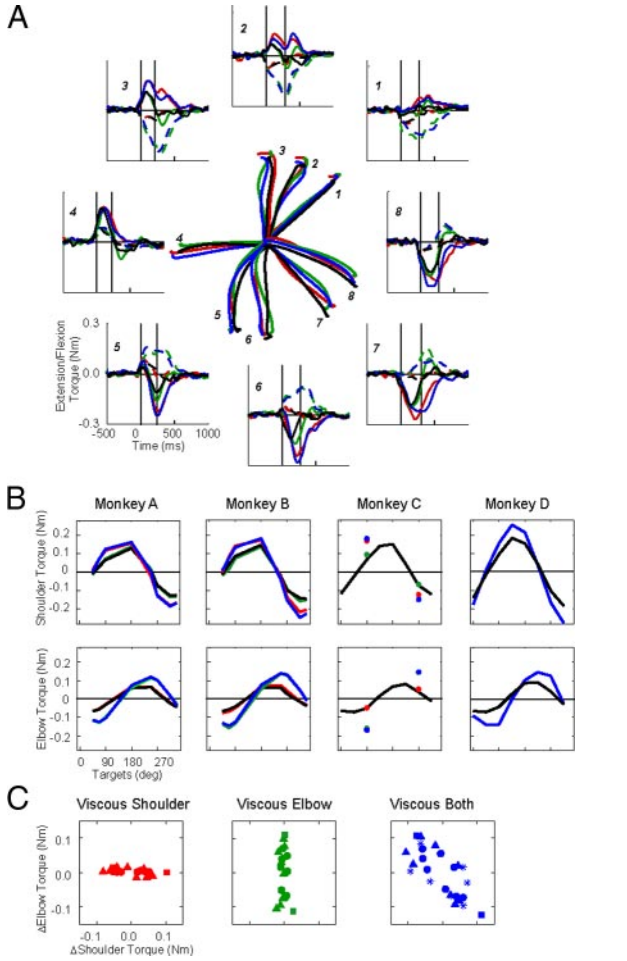

FIG. 4. Pattern of compensatory joint torque to viscous loads. *A*: *center panel* depicts the mean hand paths of a sample session (same as Fig. 1*B*). Different colors denote the different load conditions: unloaded (black), viscous shoulder (red), viscous elbow (green), and viscous shoulder (blue). *Peripheral panels* show the mean torque profiles of the shoulder (solid) and elbow (dashed) from the same session. First vertical lines in each panel indicate the time of movement onset, whereas the 2nd vertical lines indicate the time of peak velocity averaged across load conditions. *B*: each panel depicts the mean torque for one monkey and one joint (see METHODS, *Task and apparatus*). *C*: each panel depicts the change in shoulder and elbow torque between unloaded and loaded conditions. Circles, squares, triangles, and stars denote monkeys A–D.

To achieve similar movement patterns, the monkeys selectively countered the viscous loads. The change in torque was primarily at the shoulder during the viscous-shoulder condition and at the elbow during the viscous-elbow condition (Fig. 4*C*). The change in shoulder torque in the viscous-both condition was nearly identical to the combined change in shoulder torque from the viscous-shoulder and viscous-elbow conditions: shoulder torque, $r = 0.98$. The change in elbow torque was also highly predictable between single-joint and multijoint conditions, $r = 0.99$ (Fig. 4*B*). Different values for each monkey reflect their different limb geometries and different targets used.

Reach-related activity of shoulder and elbow muscles

During unloaded reaching the upper arm muscles were maximally active for a single direction of hand motion (mus-

cle's PHD = 271°, $P < 0.01$) (Fig. 5*A*). Such tuning was required for our selection criterion, but was also a typical pattern (Flanders et al. 1991; Hoffman and Strick 1999; Scott and Kalaska 1997; Turner et al. 1995). Elbow flexors and extensors expressed PHDs strongly oriented toward (mean PHD = 268°) and away from (mean PHD = 98°) the body, respectively (Fig. 6). The PHDs of shoulder flexors and extensors were oriented mostly away-left (mean PHD = 114°) and mostly toward-right (mean PHD = 305°) (Fig. 6). Last, biarticular extensors and flexors formed two clusters of PHDs oriented toward-left (mean PHD = 228°) and toward-right (mean PHD = 305°) rather than the opposing PHDs observed in single-joint antagonists (Fig. 6). The entire set of sampled muscles had a weak unimodal distribution ($P = 0.05$) and a negligible quadrimodal distribution ($P > 0.2$). In contrast, the group expressed a strong bimodal distribution that approached the fore–aft axis (PHA = 102–282°, Rayleigh test, $P < 0.001$) (Fig. 7*A*).

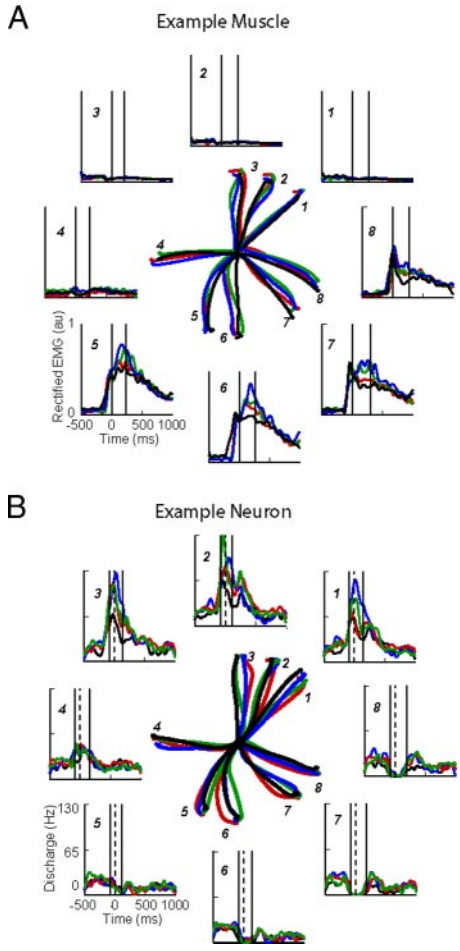

FIG. 5. Reach-related activity of a sample muscle and sample neuron. *A*: *peripheral panels* show the mean electromyographic (EMG) profile of a sample elbow flexor (brachioradialis: monkey B–acute) during reaching movements to different targets. Solid vertical lines denote time window used for analysis (movement onset to peak velocity). Colors denote load conditions as in Fig. 4. *Central panel*: mean hand paths of a sample session (same as Fig. 1*B*). *B*: *peripheral* and *central panels* show sample neural activation and hand paths from a sample session (different session than *A*) in the same format as above. Solid vertical lines denote time window used for analysis (75 ms before movement onset to 75 ms before peak velocity). Dashed vertical lines denote movement onset.

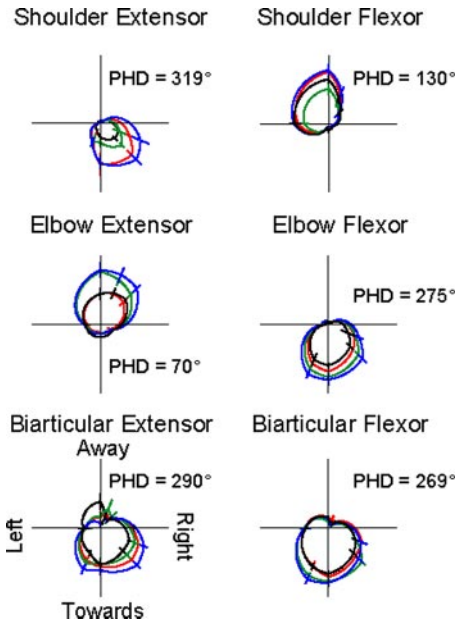

FIG. 6. Reach-related activity in each muscle group. Each panel shows a sample muscle from the 6 different muscle groups: shoulder extensors (posterior deltoid: monkey B–acute), shoulder flexors (anterior deltoid: monkey A–chronic), elbow extensors (triceps medial: monkey A–acute), elbow flexors (brachioradialis: monkey B–acute), biarticular extensors (triceps long: monkey B–acute), and biarticular flexors (biceps long: monkey B–acute). Distance from the origin indicates the mean EMG ∀ SD (normalized units) during reaching movements to different targets. Colors denote load conditions as in Fig. 4.

Torque-related activity of shoulder and elbow muscles

Arm muscles typically displayed a different pattern of activity between unloaded and loaded conditions. The interrelation between movement, torque, and EMG activity is elaborated for a sample muscle (elbow flexor) (Fig. 8, *A–D*). Here we focus on the target nearest its unloaded PHD where its load-related modulation is greatest. During the viscous-shoulder and viscous-elbow conditions the monkey generated additional shoulder-extension and elbow-flexion torques to achieve a similar movement pattern. The muscle's EMG was elevated from its activity during unloaded reaching in both cases and was greater still during the viscous-both condition. Conse-

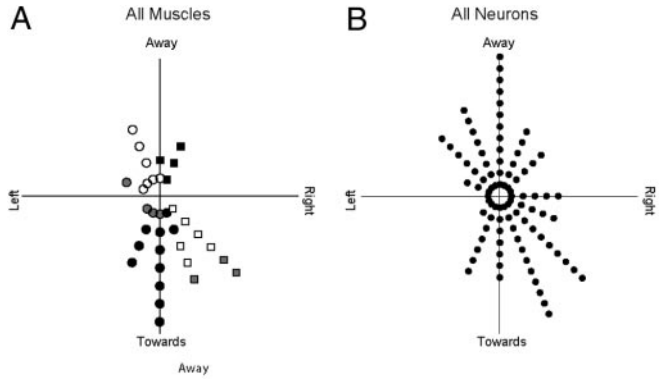

FIG. 7. Preferred hand direction (PHD) of all muscles and neurons. *A*: polar histogram summarizes the PHDs from all sampled muscles. Each muscle's PHD is represented by a single icon within an angular bin (16 bins of 22.5°). White, black, and gray symbols indicate shoulder monoarticulars, elbow monoarticulars, and biarticulars; circles and squares indicate flexors and extensors. *B*: polar histogram of PHDs from all sampled neurons.

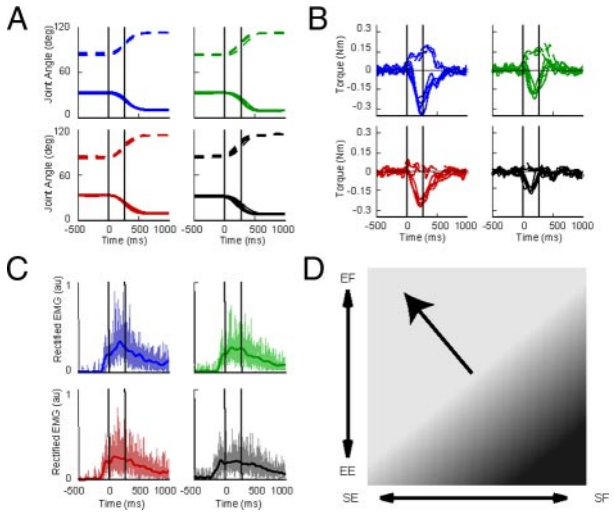

FIG. 8. Relation between joint motion, joint torque, and EMG. *A*: joint motion of the shoulder (solid) and elbow (dashed) for target 6 in Fig. 5*A*. This target is nearest the preferred torque direction (PTD) of the sample muscle. Colors denote load conditions as in Fig. 4. *B*: joint torque from the same session. *C*: rectified EMG from the same session. *D*: planar fit of the change in EMG vs. the change in joint torque; the absolute change is represented by the gray-scale gradient (lighter shade indicates greater activity). Thick arrow indicates the PTD.

quently, a planar regression of the change in activity versus the change in torque indicated a preferred torque direction of 130 ∀ 8° ($P < 0.01$).

Torque-related activity was observed for most muscles (83%) and in each muscle group (Figs. 6 and 9). Torque-related changes were mostly increases from the activity during unloaded reaching (median loaded-EI score = 0.75); the maximum change was roughly 80% of the maximum unloaded activity. Importantly, the preferred torque direction of a muscle often differed from its anatomical action. For example, the elbow flexor shown in Fig. 8 increased its activity with both elbow flexor torque and shoulder extensor torque, even though it was a single-joint muscle (measured = 130° vs. expected = 90°). Significant PTD biases from anatomical action were observed for nearly half the muscles with significant torque-related activity (Table 1). The mean bias (toward shoulder-extension/elbow-flexion torques or shoulder-flexion/elbow-extension torques) of shoulder, elbow, and biarticular muscles was, respectively, 4 ± 24° (*t*-test, $P > 0.05$), 30 ± 26° (*t*-test, $P < 0.01$), and 41 ± 18° (*t*-test, $P < 0.01$) (Fig. 10*A*). The mean bias of 22° created a significant bimodal PTD distribution toward shoulder-extension/elbow-flexion torque and shoulder-flexion/elbow-extension torque (147–327°, Rayleigh test, $P = 0.015$) (Fig. 10*C*). A significant quadrimodal trend of the group was also observed ($P = 0.01$), whereas a unimodal trend was weak ($P = 0.08$). The significant quadrimodal distribution reflects that the mean PTD rotation was 22° and that the bimodal axis 145–327° does not match the modal vector (see METHODS).

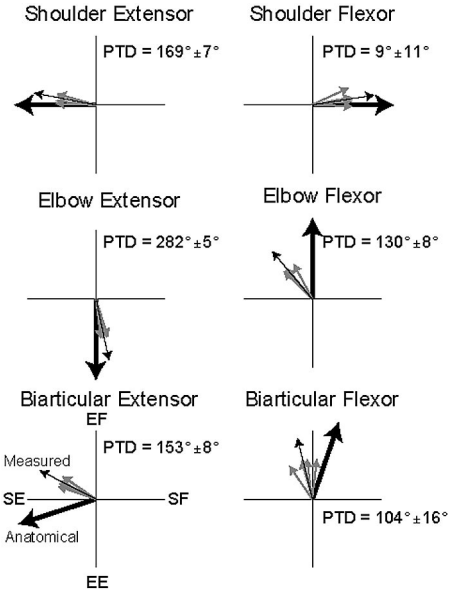

FIG. 9. Torque-related activity of each muscle group. Each panel shows a sample muscle from the 6 different muscle groups (same sample muscles from Fig. 6). Torque coordinate frame with shoulder flexion, elbow flexion, shoulder extension, and elbow extension starts at 0° and increases counterclockwise. Small gray arrows indicate the PTDs of the 5 repeat blocks, thin black arrows indicate the measured PTD, and thick black arrows indicate the expected PTD based on anatomy. Expected PTD of a monoarticular muscle is restricted to the axis for shoulder torque or elbow torque.

Reach-related and torque-related activity of cortical neurons

The sample neuron of Fig. 5*B* displays several features commonly observed in M1 neurons (and arm muscles). Fore-

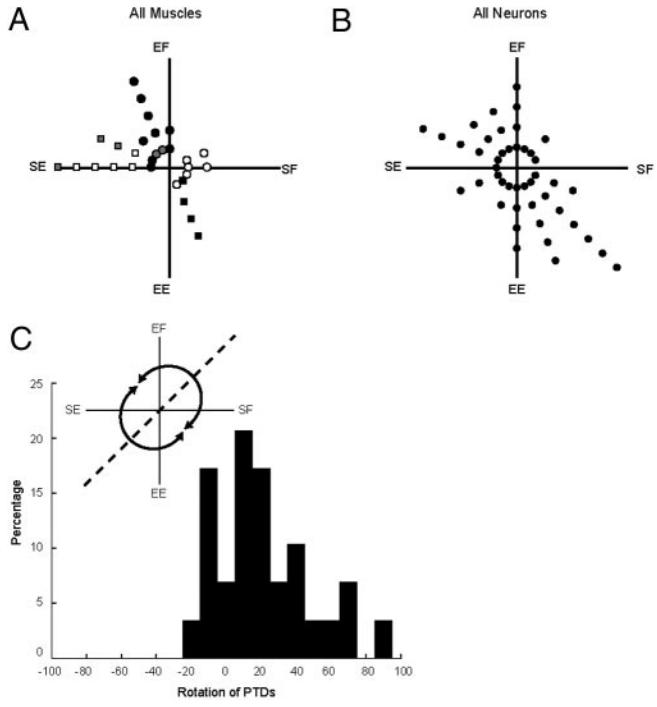

FIG. 10. PTD of all muscles and neurons. *A*: polar histogram depicts the PTDs for all muscle samples (grouped into 16 bins of 22.5°). White, black, and gray symbols indicate shoulder monoarticulars, elbow monoarticulars, and biarticulars; circles and squares indicate flexors and extensors. *B*: polar histogram of PTDs from all sampled neurons (16 bins of 22.5°). *C*: histogram of the muscles' PTD rotating toward (positive) and away (negative) from shoulder-extension/elbow-flexion or shoulder-flexion/elbow-extension. Width of each bar is 10°. *Inset*: definition of direction of PTD rotation. Orientation of a muscle's moment arm determined whether a clockwise or counterclockwise rotation of its PTD (switches along 45–225° axis) approaches the quadrants for shoulder-extension/elbow-flexion or shoulder-flexion/elbow-extension. Rotations in this manner were considered positive; otherwise, rotations were considered negative.

most, the neuron exhibited significant directional tuning during unloaded reaching (PHD = 90°, $P < 0.01$). Roughly 70% of neurons expressed unimodal tuning from a larger sample ($n = 493$) selected under relatively liberal criteria—modulated by passive movements, postural loads, and perturbations during posture or reaching movements. Moreover, the PHDs of neurons (like muscles) formed a strongly bimodal distribution bias that approached the fore–aft axis (PHA = 109–289°, Rayleigh test, $P < 0.001$) (Fig. 7*B*) (Scott et al. 2001); the distribution was not significantly unimodal ($P > 0.2$) or quadrimodal ($P > 0.1$). Bootstrap tests indicated no significant difference between the bimodal spatial orientation of arm muscles and arm-related neurons ($P > 0.05$).

The sample neuron of Fig. 5*B* also showed changes in activity related to the change in torque (PTD = 292 ∀ 15°, $P < 0.01$). Torque-related changes were common in M1 neurons and represented a significant fraction of the activity during unloaded reaching; the maximum change was nearly 76% of the maximum unloaded activity on average. Moreover, the entire sample of M1 neurons showed a strongly bimodal distribution of PTDs toward shoulder-extension/elbow-flexion torque and shoulder-flexion/elbow-extension torque (125–305°, Rayleigh test, $P < 0.01$) (Fig. 10*B*); the distribution was not significantly unimodal ($P > 0.2$) or quadrimodal ($P > 0.2$). Further, bootstrap tests indicated no significant difference between the bimodal torque orientation of muscles and neurons ($P > 0.05$).

Although M1 neurons and muscles shared several key features, they did not exhibit identical patterns. For example, during unloaded reaching the neurons showed greater decreases from prereach activity than observed in muscles (median unloaded-EI score: muscles = 0.97 vs. neurons = 0.73; Wilcoxon test, $P < 0.05$). Torque-related activity was also less common than that in muscles (proportion: muscle = 83% vs. neuron = 50%; difference of proportions, $P < 0.01$). Last, the torque-related changes in M1 neurons involved equal increases and decreases relative to the activity during unloaded reaching, whereas muscles showed significantly more increases than decreases (median loaded-EI score: muscles = 0.75 vs. neurons = 0.03; Wilcoxon test, $P < 0.01$).

Models of muscle activation

We found that both muscle properties and the recruitment strategy could affect the modeled PHDs. The simplest case is the "direct activation" model without any length- and velocity-dependent muscle properties. This arrangement predicts that the PHDs of single-joint muscles mirror the torque of their spanned joint (compare Fig. 2*C* with Fig. 11*A*). Likewise, biarticular PHDs reflect a combination of shoulder and elbow torque in proportion to their anatomical contribution. Therefore the "direct activation" model incorrectly predicts *1*) that the PHDs of all muscle groups are biased to the left–right axis (PHA = 174–354°) and *2*) that biarticulars have nearly opposite PHDs (Fig. 11, *A* and *B*).

The addition of length- and velocity-dependent muscle properties required greater muscle activation along the fore–aft axis where the joint motion and displacement were greatest (Fig. 2*C*). Passive stiffness required a 7 and 18% increase, respectively, in activation of shoulder and elbow muscles from their

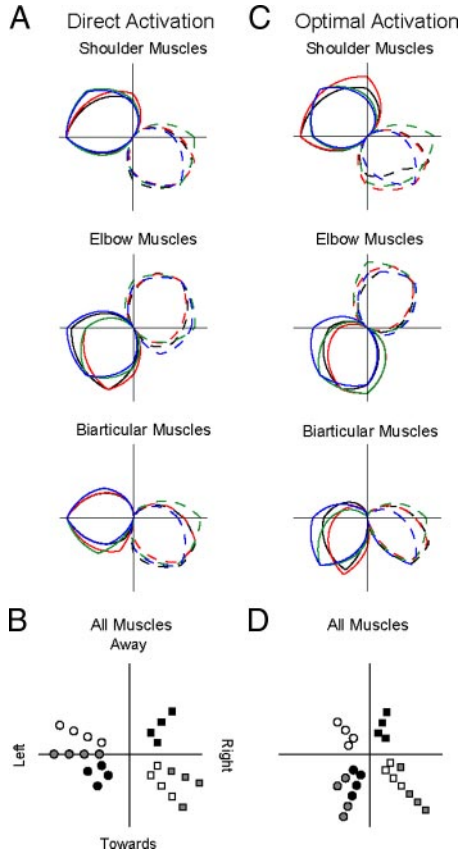

FIG. 11. Reach-related activity predicted by the muscle models. *A*: predicted activity from the "direct activation" model that lacks muscle stiffness and damping. Each muscle group is represented 4 times, once for each monkey. Solid and dashed lines denote activity of the flexors and extensors, respectively. *B*: polar histogram of the predicted PHDs; symbols same as Fig. 7. *C*: predicted activity from the "optimal activation" model that includes stiffness and damping. *D*: polar histogram of the predicted PHDs.

previous maximum. The influence of muscle velocity required a maximum increase of 30 and 35% from the peak shoulder torque and peak elbow torque, respectively. Thereby, muscle stiffness and damping induced a mean rotation of 3 and 6°, respectively, toward the fore–aft axis (*t*-test, $P < 0.01$). Optimizing the muscle activation also affected the PHDs (mean rotation = 11°, $P < 0.01$). Further, muscle stiffness, muscle damping, and optimal activation have a larger cumulative influence than that of any single factor (mean rotation of full model = 19°, *t*-test, $P < 0.01$) and are sufficient to induce a fore–aft orientation of the entire sample of PHDs (PHA = 105–285°), although less than experimentally observed (Figs. 7*A* and 11, *C* and *D*).

We modeled the muscle activation during both unloaded and loaded conditions. Similar to our observations the modeled muscles showed increases in activity with increased load that were nearly collinear with the unloaded baseline (compare Fig. 6*A* with Fig. 12*A*). We examined the models' PTDs under a variety of conditions: with/without muscle intrinsic properties, with identical or measured movement patterns, and with/without the optimal muscle activation. The most complex "direct activation" model—with muscle intrinsic properties and measured movement patterns—did not show a significant PTD rotation toward shoulder-flexion/elbow-extension torque and shoulder-extension/elbow-flexion torque (mean = −2°,

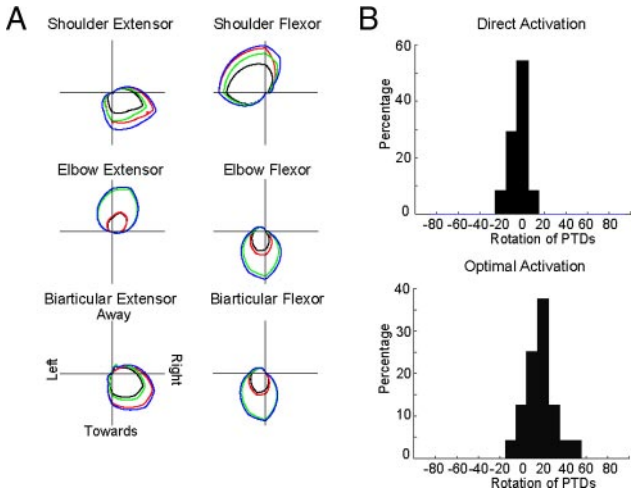

FIG. 12. Torque-related activity predicted by the muscle models. *A*: sample activity of each muscle group from one monkey. Predictions from the "optimal activation" model that includes muscle stiffness and damping. Colors denote the 4 load conditions as in Fig. 4. *B*: histogram of PTD rotations from the "direct activation" and "optimal activation" models. Both include muscle stiffness and damping.

t-test, $P > 0.05$). In fact, significant PTD rotation occurred only with the optimal activation strategy (mean = 17°, *t*-test, $P < 0.01$) (compare Fig. 10*C* with Fig. 12*B*). This effect was robust over a range of simulated movement speeds (halved and doubled) and different cost functions.

DISCUSSION

Paradigm of loaded reaching

A major concern in motor control is to understand the muscle patterns that underlie movement (Zajac and Gordon 1989). In studies of reaching movements, researchers often implicitly vary the muscular requirement of the task (for review, see Berardelli et al. 1996). Experimental manipulations include different movement speeds (Corcos et al. 1989), movement distances (Brown and Cooke 1981), movement directions (Flanders et al. 1991; Karst and Hasan 1991; Scott and Kalaska 1997; Turner et al. 1995), and applied loads (Gottlieb 1996). Such studies provide insight into the flexibility of activation patterns but cannot (nor are intended to) examine how muscle activity is specifically related to joint torque.

In the present study we enforced similar limb movements during the application of different joint-based loads. This paradigm is analogous to muscular studies of postural control where the limb's configuration is constant during torque production (Buchanan et al. 1989; Kurtzer et al. 2006; Nozaki et al. 2005; Theeuwen et al. 1994). Muscle activation during these two tasks is fundamentally different because posture involves tonic activity and movement requires complex spatiotemporal patterns correlated to the extrinsic load and intrinsic muscle properties. However, enforcing similar movements with and without loads allowed us to peel away the unloaded reach-related activity and examine how muscle activity is specifically related to multijoint torque.

The loaded-reaching paradigm has several limitations arising from the velocity dependency of muscle and use of velocity-dependent loads. First, the impact on muscle force production resulting from shortening velocity varies across muscles because of their differing fascicle lengths, fiber type, and moment arms (Graham et al. 2003b; Singh et al. 2002). However, the velocity profile of each muscle will be approximately constant across loads if the movement pattern is conserved. Second, to reliably obtain similar limb trajectories across load conditions we enforced a movement speed below the animal's unloaded preference and above their loaded preference. This resulted in consistent performance but without a strong antagonist burst. Our modeling results suggest that similar patterns of torque-related activity occur over a range of movement speeds. Last, the load paradigm applied a nonuniform distribution of joint torques arising from the nonuniform relation between joint velocity and hand motion. The most frequent and largest torques involved shoulder-extension/elbow-flexion torque and shoulder-flexion/elbow-extension torque rather than flexion/flexion or extension/extension. We partly addressed this problem with a planar regression because it can readily handle nonuniform and unequal samples. Our modeling effort further confirmed that our uneven sampling per se did not systematically misestimate the PTDs because biases did not occur with the direct activation model. Future studies using a different applied load (such as a constant load) may allow faster movements with an antagonist burst and more uniform sampling of joint torque.

Muscular bias in PTDs and PHDs

During loaded reaching, the arm muscles exhibited a bias in their PTDs toward shoulder-flexion/elbow-extension torque and shoulder-extension/elbow-flexion torque. The resulting bimodal distribution in torque space could be considered evidence of functional grouping of muscles such as whole-arm flexion and extension synergies. Similar synergies were previously suggested to underlie motor behavior (Bernstein 1967; d'Avella et al. 2003; Ivanenko et al. 2004; MacPherson 1986; Ting and MacPherson 2005). However, we could reproduce the PTD bias using an optimization model that lacked any explicit grouping of muscles (Fagg et al. 2002; Kurtzer et al. 2006; Nozaki et al. 2005; van Bolhuis and Gielen 1999). [Note that PTD biases can result from other constraints on the motor system (besides optimization) such as cosine tuning to torque (Nozaki et al. 2005).] By examining the model with and without biarticular muscles we discounted that the PTD bias was an artifact of nonuniformities in the torques and/or small differences in movement patterns between load conditions. Rather, PTD biases reflect the interactions within a redundant muscle system.

During unloaded center-out reaching, we observed a strong bias in the muscles' preferred hand direction to targets located toward and away from the body. The bias in PHDs likely reflects three separate factors: limb geometry, muscle mechanics, and the bias of PTDs. If arm muscles were pure torque generators, the required muscular torque would be biased to the left and right of the body (see *Models of muscle activation* in RESULTS). However, the limb's geometry ensures that the largest joint velocities (and thus muscle velocity and displacement) occur toward and away from the body (Graham et al. 2003a). This meant that the greatest compensation for intrinsic damping and stiffness (Joyce et al. 1969; Scott et al. 1996) occurred along the fore–aft orientation. Last, the bias of muscles' PTDs (Kurtzer et al. 2006) will similarly bias the PHDs because

shoulder-flexion/elbow-extension torque and shoulder-extension/elbow-flexion torque (where the muscle activity is greatest) occur with movements toward and away from the body, respectively. The efficacy of each separate factor was confirmed with a model of muscle activation.

In contrast to the present study, previous investigations have not reported a strong bias in the muscle's distribution of PHDs. However, these previous studies required abduction/adduction and internal/external rotation of the limb in addition to shoulder and elbow flexion/extension (Georgopoulos et al. 1982; Kalaska et al. 1989; Moran and Schwartz 1999; Scott and Kalaska 1997; Sergio and Kalaska 2005). Use of these degrees of freedom will certainly involve different muscle patterns. Second, these studies used unsupported limb movements that require greater muscle activity for movements away from the body resulting from the influence of gravity (Moran and Schwartz 1999). Finally, previous studies often used handheld pendula (Kalaska et al. 1989; Scott and Kalaska 1997; Sergio and Kalaska 2005) that will inflate the required muscular torques for left–right movements versus fore–aft movements arising from different mechanical advantages in the two directions. In contrast, the robotic exoskeleton used in the present study constrained the entire limb to a single plane, removed the influence of gravity, and had an inertial distribution roughly aligned with the animal's limb (Scott 1999).

Comparing muscular and M1 activity patterns

The observed patterns of muscular activity during reaching provide a foundation for interpreting cortical function in the same task. In particular, numerous studies have shown an intimate relationship between M1 and the motor periphery, including a dense descending projection to segmental regions (Dum and Strick 1991; Porter and Lemon 1993), with some direct input to motor neurons (Fetz and Cheney 1987; Lemon and Griffiths 2005). Moreover, the discharges of individual M1 neurons often covary with the mechanical attributes of a task and underlying muscular activity (Ashe 1997; Drew et al. 2004; Evarts 1968; Holdefer and Miller 2002; Lamarre et al. 1981).

Other studies have examined M1's relation to the motor periphery by considering all the muscles or neurons together. As a population, both arm muscles and arm-related M1 neurons exhibit a coupling between their onset time and magnitude of response (Scott 1997). Both rotate their PHDs (Caminiti et al. 1990; Scott and Kalaska 1997) and load sensitivities (Sergio and Kalaska 2003) with rotations about the shoulder (for rotations of preferred wrist direction, see Kakei et al. 1999). Both show similar temporal changes in their global preferred direction during reaching movements (Sergio and Kalaska 2005; Todorov 2000). Last, both muscles and M1 neurons are biased toward whole-arm flexion and whole-arm extension torques during a posture task (Cabel et al. 2001; Kurtzer et al. 2006).

The present data add to this list of population similarities in two ways. First, during unloaded center-out reaching the muscles' PHDs were strongly biased along an axis toward–away from the body as observed in the M1 neurons from the same monkeys (Scott et al. 2001). Second, the PTDs of arm muscles were biased toward shoulder-extension/elbow-flexion torque and shoulder-flexion/elbow-extension torque, again like M1 neurons from the same monkeys.

The similarities between M1 and muscular patterns do not imply a one-to-one mapping. Anatomically, M1 projects broadly to spinal lamina involved in different sensorimotor functions (Porter and Lemon 1993). Moreover, previous studies showed that M1 neurons show an impressive degree of variety, plasticity, and context dependency not present in limb muscles (Kakei et al. 1999; Kurtzer et al. 2005; Li et al. 2001; Paz et al. 2004; Sanes and Donoghue 2000; Scott 2003). In the present study, one clear difference between upper limb muscles and M1 neurons is the higher frequency of load-related activity in muscles; roughly half the neurons did not show load-related activity. Therefore many aspects of M1 function illustrate its role for converting global goals into detailed motor plans but also indicate it is not merely a collection of upper motor neurons. This association of low-level specificity with context-dependent processing is consistent with M1 playing a pivotal role within a motor system that behaves like an optimal feedback controller (Scott 2004; Todorov and Jordan 2002).

ACKNOWLEDGMENTS

The authors thank K. Moore and J. Swaine for technical support and A. Coderre, G. King, and J. A Pruszynski for critical reading.

GRANTS

The present research was supported by Canadian Institute of Health Research (CIHR) grants and a CIHR Investigator award to S. H. Scott.

REFERENCES

Ashe J. Force and the motor cortex. *Behav Brain Res* 87: 255–269, 1997.

Batschelet E. *Circular Statistics in Biology.* New York: Academic Press, 1981.

Berardelli A, Hallett M, Rothwell JC, Agostino R, Manfredi M, Thompson PD, and Marsden CD. Single-joint rapid arm movements in normal subjects and in patients with motor disorders. *Brain* 119: 661–674, 1996.

Bernstein NA. *The Coordination and Regulation of Movements.* Oxford, UK: Pergamon Press, 1967.

Brown SH and Cooke JD. Amplitude- and instruction-dependent modulation of movement-related electromyogram activity in humans. *J Physiol* 316: 97–107, 1981.

Buchanan TS, Rovai GP, and Rymer WZ. Strategies for muscle activation during isometric torque generation at the human elbow. *J Neurophysiol* 62: 1201–1212, 1989.

Cabel DW, Cisek P, and Scott SH. Neural activity in primary motor cortex related to mechanical loads applied to the shoulder and elbow during a postural task. *J Neurophysiol* 86: 2102–2108, 2001.

Caminiti R, Johnson PB, and Urbano A. Making arm movements within different parts of space: dynamic aspects in the primate motor cortex. *J Neurosci* 10: 2039–2058, 1990.

Cheney PD, Mewes K, and Fetz EE. Encoding of motor parameters by corticomotoneuronal (CM) and rubromotoneuronal (RM) cells producing postspike facilitation of forelimb muscles in the behaving monkey. *Behav Brain Res* 28: 181–191, 1988.

Cheng EJ and Scott SH. Morphometry of *Macaca mulatta* forelimb. I. Shoulder and elbow muscles and segment inertial parameters. *J Morphol* 245: 206–224, 2000.

Collins JJ. The redundant nature of locomotor optimization laws. *J Biomech* 28: 251–267, 1995.

Corcos DM, Gottlieb GL, and Agarwal GC. Organizing principles for single-joint movements. II. A speed-sensitive strategy. *J Neurophysiol* 62: 358–368, 1989.

Crowninshield RD and Brand RA. A physiologically based criterion of muscle force prediction in locomotion. *J Biomech* 14: 793–801, 1981.

d'Avella A, Saltiel P, and Bizzi E. Combinations of muscle synergies in the construction of a natural motor behavior. *Nat Neurosci* 6: 300–308, 2003.

Drew T, Prentice S, and Schepens B. Cortical and brainstem control of locomotion. *Prog Brain Res* 143: 251–261, 2004.

Dul J, Johnson GE, Shiavi R, and Townsend MA. Muscular synergism—II. A minimum-fatigue criterion for load sharing between synergistic muscles. *J Biomech* 17: 675–684, 1984.

Dum RP and Strick PL. The origin of corticospinal projections from the premotor areas in the frontal lobe. *J Neurosci* 11: 667–689, 1991.

Evarts EV. Relation of pyramidal tract activity to force exerted during voluntary movement. *J Neurophysiol* 31: 14–27, 1968.

Fagg AH, Shah A, and Barto AG. A computational model of muscle recruitment for wrist movements. *J Neurophysiol* 88: 3348–3358, 2002.

Fetz EE and Cheney PD. Functional relations between primate motor cortex cells and muscles: fixed and flexible. *Ciba Found Symp* 132: 98–117, 1987.

Flanders M. Temporal patterns of muscle activation for arm movements in three-dimensional space. *J Neurosci* 11: 2680–2693, 1991.

Georgopoulos AP, Kalaska JF, Caminiti R, and Massey JT. On the relations between the direction of two-dimensional arm movements and cell discharge in primate motor cortex. *J Neurosci* 2: 1527–1537, 1982.

Gottlieb GL. On the voluntary movement of compliant (inertial-viscoelastic) loads by parcellated control mechanisms. *J Neurophysiol* 76: 3207–3229, 1996.

Graham KM, Moore KD, Cabel DW, Gribble PL, Cisek P, and Scott SH. Kinematics and kinetics of multijoint reaching in nonhuman primates. *J Neurophysiol* 89: 2667–2677, 2003a.

Graham KM and Scott SH. Morphometry of *Macaca mulatta* forelimb. III. Moment arm of shoulder and elbow muscles. *J Morphol* 255: 301–314, 2003b.

Gribble PL and Scott SH. Method for assessing directional characteristics of non-uniformly sampled neural activity. *J Neurosci Methods* 113: 187–197, 2002a.

Gribble PL and Scott SH. Overlap of internal models in motor cortex for mechanical loads during reaching. *Nature* 417: 938–941, 2002b.

Haruno M and Wolpert DM. Optimal control of redundant muscles in step-tracking wrist movements. *J Neurophysiol* 94: 4244–4255, 2005.

Hepp-Reymond M. Functional organization of motor cortex and its participation in voluntary movements. In: *Comparative Primate Biology*, edited by Alan R. New York: Liss, 1988, p. 501–624.

Hoffman DS and Strick PL. Step-tracking movements of the wrist. IV. Muscle activity associated with movements in different directions. *J Neurophysiol* 81: 319–333, 1999.

Holdefer RN and Miller LE. Primary motor cortical neurons encode functional muscle synergies. *Exp Brain Res* 146: 233–243, 2002.

Hollerbach JM and Flash T. Dynamic interactions between limb segments during planar arm movement. *Biol Cybern* 44: 67–77, 1982.

Ivanenko YP, Poppele RE, and Lacquaniti F. Five basic muscle activation patterns account for muscle activity during human locomotion. *J Physiol* 556: 267–282, 2004.

Jongen HA, Denier van der Gon JJ, and Gielen CC. Activation of human arm muscles during flexion/extension and supination/pronation tasks: a theory on muscle coordination. *Biol Cybern* 61: 1–9, 1989.

Joyce GC, Rack PM, and Westbury DR. The mechanical properties of cat soleus muscle during controlled lengthening and shortening movements. *J Physiol* 204: 461–474, 1969.

Kakei S, Hoffman DS, and Strick PL. Muscle and movement representations in the primary motor cortex. *Science* 285: 2136–2139, 1999.

Kalaska JF, Cohen DA, Hyde ML, and Prud'homme M. A comparison of movement direction-related versus load direction-related activity in primate motor cortex, using a two-dimensional reaching task. *J Neurosci* 9: 2080–2102, 1989.

Karst GM and Hasan Z. Timing and magnitude of electromyographic activity for two-joint arm movements in different directions. *J Neurophysiol* 66: 1594–1604, 1991.

Kurtzer I, Herter TM, and Scott SH. Random change in cortical load representation suggests distinct control of posture and movement. *Nat Neurosci* 8: 498–504, 2005.

Kurtzer I, Pruszynski JA, Herter TM, and Scott SH. Primate upper limb muscles exhibit activity patterns that differ from their anatomical action during a postural task. *J Neurophysiol* 95: 493–504, 2006.

Lamarre Y, Spidalieri G, and Lund JP. Patterns of muscular and motor cortical activity during a simple arm movement in the monkey. *Can J Physiol Pharmacol* 59: 748–756, 1981.

Lemon RN and Griffiths J. Comparing the function of the corticospinal system in different species: organizational differences for motor specialization? *Muscle Nerve* 32: 261–279, 2005.

Li CS, Padoa-Schioppa C, and Bizzi E. Neuronal correlates of motor performance and motor learning in the primary motor cortex of monkeys adapting to an external force field. *Neuron* 30: 593–607, 2001.

Loeb GE, Brown IE, and Cheng EJ. A hierarchical foundation for models of sensorimotor control. *Exp Brain Res* 126: 1–18, 1999.

Loeb GE and Gans C. *Electromyography for Experimentalists.* London: Univ. of Chicago Press, 1986.

Macpherson JM, Rushmer DS, and Dunbar DC. Postural responses in the cat to unexpected rotations of the supporting surface: evidence for a centrally generated synergic organization. *Exp Brain Res* 62: 152–160, 1986.

Moran DW and Schwartz AB. Motor cortical representation of speed and direction during reaching. *J Neurophysiol* 82: 2676–2692, 1999.

Morasso P. Spatial control of arm movements. *Exp Brain Res* 42: 223–227, 1981.

Morrow MM and Miller LE. Prediction of muscle activity by populations of sequentially recorded primary motor cortex neurons. *J Neurophysiol* 89: 2279–2288, 2003.

Nozaki D, Nakazawa K, and Akai M. Muscle activity determined by cosine tuning with a nontrivial preferred direction during isometric force exertion by lower limb. *J Neurophysiol* 93: 2614–2624, 2005.

Paz R, Wise SP, and Vaadia E. Viewing and doing: similar cortical mechanisms for perceptual and motor learning. *Trends Neurosci* 27: 496–503, 2004.

Porter R and Lemon RN. *Corticospinal Function and Voluntary Movement.* New York: Oxford Univ. Press, 1993.

Sanes JN and Donoghue JP. Plasticity and primary motor cortex. *Annu Rev Neurosci* 23: 393–415, 2000.

Scott SH. Apparatus for measuring and perturbing shoulder and elbow joint positions and torques during reaching. *J Neurosci Methods* 89: 119–127, 1999.

Scott SH. The role of primary motor cortex in goal-directed movements: insights from neurophysiological studies on non-human primates. *Curr Opin Neurobiol* 13: 671–677, 2003.

Scott SH. Optimal feedback control and the neural basis of volitional motor control. *Nat Rev Neurosci* 5: 532–546, 2004.

Scott SH, Brown IE, and Loeb GE. Mechanics of feline soleus: I. Effect of fascicle length and velocity on force output. *J Muscle Res Cell Motil* 17: 207–219, 1996.

Scott SH, Gribble PL, Graham KM, and Cabel DW. Dissociation between hand motion and population vectors from neural activity in motor cortex. *Nature* 413: 161–165, 2001.

Scott SH and Kalaska JF. Reaching movements with similar hand paths but different arm orientations. I. Activity of individual cells in motor cortex. *J Neurophysiol* 77: 826–852, 1997.

Sergio LE, Hamel-Paquet C and Kalaska JF. Motor cortex neural correlates of output kinematics and kinetics during isometric force and arm-reaching tasks. *J Neurophysiol* 94: 2353–2378, 2005.

Sergio LE and Kalaska JF. Systematic changes in motor cortex cell activity with arm posture during directional isometric force generation. *J Neurophysiol* 89: 212–228, 2003.

Singh K, Melis EH, Richmond FJ, and Scott SH. Morphometry of *Macaca mulatta* forelimb. II. Fiber-type composition in shoulder and elbow muscles. *J Morphol* 251: 323–332, 2002.

Theeuwen M, Gielen CC, and Miller LE. The relative activation of muscles during isometric contractions and low-velocity movements against a load. *Exp Brain Res* 101: 493–505, 1994.

Ting LH and Macpherson JM. A limited set of muscle synergies for force control during a postural task. *J Neurophysiol* 93: 609–613, 2005.

Todorov E. Direct cortical control of muscle activation in voluntary arm movements: a model. *Nat Neurosci* 3: 391–398, 2000.

Todorov E and Jordan MI. Optimal feedback control as a theory of motor coordination. *Nat Neurosci* 5: 1226–1235, 2002.

Turner RS, Owens JW Jr, and Anderson ME. Directional variation of spatial and temporal characteristics of limb movements made by monkeys in a two-dimensional work space. *J Neurophysiol* 74: 684–697, 1995.

van Bolhuis BM and Gielen CC. A comparison of models explaining muscle activation patterns for isometric contractions. *Biol Cybern* 81: 249–261, 1999.

van Bolhuis BM, Gielen CC, and Ingen Schenau GJ. Activation patterns of mono- and bi-articular arm muscles as a function of force and movement direction of the wrist in humans. *J Physiol* 508: 313–324, 1998.

van Zuylen EJ, Gielen CC, and Denier van der Gon JJ. Coordination and inhomogeneous activation of human arm muscles during isometric torques. *J Neurophysiol* 60: 1523–1548, 1988.

Zajac FE and Gordon ME. Determining muscle's force and action in multi-articular movement. *Exerc Sport Sci Rev* 17: 187–230, 1989.